

Characterization of critical gel state of polyamides by viscoelastic, thermal, and IR measurements

<sup>1</sup>Takaya Hirayama, <sup>2</sup>Takashi Uneyama, and <sup>3</sup>Yuichi Masubuchi\*

Department of Applied Physics, Center of Computational Science, and Department of Materials Physics, Nagoya University

\*to whom correspondence should be addressed.

[mas@mp.pse.nagoya-u.ac.jp](mailto:mas@mp.pse.nagoya-u.ac.jp)

REV Jan 7, 2019

Published in Rheologica Acta, 58(5), 281-290 (2019) [doi:10.1007/s00397-019-01136-0](https://doi.org/10.1007/s00397-019-01136-0).

## ABSTRACT

We examined the liquid-solid transition for polyamides (PA) 6, 66 and 610 by the Chambon-Winter method under cooling. The polyamides exhibited the transition via the critical gel, for which the critical exponent and the stiffness were consistent with those reported under the isothermal measurements for the other polymers. The DSC measurements showed that, for a few materials, the crystallinity at the gelation  $\varphi_{\text{gel}}$  was very small. This result implies that the hydrogen bonding partially stabilizes the critical gel of such polyamides. The FT-IR measurement demonstrated that the hydrogen bonding was formed cooperatively around the gelation temperature. However, we also found that with increasing the molecular weight the gelation temperature decreased and  $\varphi_{\text{gel}}$  increased for PA6. Besides,  $\varphi_{\text{gel}}$  was smaller for PA66 and PA610 than that for PA6. The mechanism is unknown for these results that locate in the opposite side to the suggested role of hydrogen bonding.

**Keywords:** viscoelasticity, gelation, rheology, semi-crystalline polymers

## INTRODUCTION

Solidification behavior of polyamides has been widely investigated due to the industrial significance. For example, this class of polymers is used as fibers and structural materials owing to their excellent mechanical and thermal properties (Marchildon 2011). Developments of blends and composites have been being attempted as well (Fornes et al. 2001). In the processing, the material in the melt state is poured into a mold of the desired

shape, and solidified by the cooling. Phenomenologically, the temperature at which the polymer is solidified is a fundamental quantity that characterizes the liquid-solid transition and used in the processing simulations for the switching between fluent and frozen states of the material (Mannella et al. 2011a). Most of the cases, the solidification temperature of polyamides is obtained from the thermal measurements. For example, in differential scanning calorimetry (DSC) measurements, the solidification temperature is defined as the temperature at which the crystallinity starts to increase, or the exothermic signal shows a peak. This approach is reasonable since polyamides are semi-crystalline polymers and the primary mechanism of the solidification is regarded as the crystallization. However, the solidification temperature determined by the thermal measurement does not correspond to the solidification temperature in a rheological sense (Mannella et al. 2011b). For instance, semi-crystalline polymers flow even including some crystallites (Tanner 2002; Watanabe et al. 2003).

Rheologically, a reasonable definition of the liquid-solid transition is the formation of a percolated network via the crystallites that play the role as the network nodes, analogous to polymer gels (Winter and Mours 1997). Winter and Chambon (Winter and Chambon 1986; Chambon and Winter 1987) used rheometers to determine the critical gel state, at which the polymer network is percolated. In their method, at the critical gel state, the storage  $G'(\omega)$  and loss moduli  $G''(\omega)$  are the power functions of the frequency  $\omega$  with the same power exponent, which is related to the fractal dimension of the network (Muthukumar and Winter 1986; Hess et al. 1988; Muthukumar 1989). This approach has been subsequently extended to semi-crystalline polymers such as polypropylene (Lin et al. 1991; Schwittay et al. 1995; Boutahar et al. 1998; Pogodina and Winter 1998; Pogodina et al. 1999, 2001), bacterial elastomer (Richtering et al. 1992), poly(1-butene) (Acierno et al. 2002; Coppola et al. 2006), polycaprolactone (Izuka et al. 1992; Acierno et al. 2006), and thermoplastic polyurethanes (Nichetti et al. 2005).

Although the studies mentioned in the previous paragraph were performed for the isothermal measurements, the viscoelastic method has also been applied to the non-isothermal solidifications. As carefully analyzed by Mours and Winter (Mours and Winter 1994), the viscoelastic method is applicable only when the rate of change of the specimen (which is so-called the mutation rate) is sufficiently smaller than  $\omega$  used for the measurement. This requirement would be fulfilled even under non-isothermal measurements unless the change in the material occurs sharply against the modulation of temperature. Under such a condition, the critical gel formation during the non-isothermal solidification has been studied for polycarbonate (via the glass transition) (Mours and Henning Winter 1995), ethylene-hexene copolymers (Gelfer et al. 2003), and

cellulose/silk-fibroin blends (Yao et al. 2014).

In this paper, we investigated the non-isothermal solidification of some polyamides by the viscoelastic method. After discussing the adequate experimental conditions, we obtained the characteristics of the critical gels. For the verification of our measurements, we examined the consistency with the earlier results reported for the isothermal solidifications of the other polymers. We also performed DSC measurements to estimate the degree of crystallinity in the critical gel to show that some polyamides solidify with small degrees of crystallinity. The additional infrared absorption (IR) measurements imply that for such cases the critical gel states are stabilized by hydrogen bonding before the crystallization. We discussed the effects of the molecular weight and the density of hydrogen bonding as well. Details are shown below.

## EXPERIMENTAL

### Materials

The materials used in this study were mainly poly(hexano-6-lactam) (PA6) of various molecular weights. The other polyamides, PA66 and 610 were also measured for comparison. All the polymers are commercially available, and their molecular weights and the distributions obtained by GPC are summarized in Table I.

Table 1 Examined samples

| Code    | Material                       | $M_w$ ( $\times 10^3$ )* | $M_w/M_n$ |
|---------|--------------------------------|--------------------------|-----------|
| PA6/40  |                                | 40                       | 5         |
| PA6/50  | poly(hexano-6-lactam)          | 50                       | 5         |
| PA6/70  |                                | 70                       | 5         |
| PA6/110 |                                | 110                      | 5         |
| PA66    | poly(hexamethylene adipamide)  | 70                       | 3         |
| PA610   | poly(hexamethylene sebacamide) | 55                       | 3         |

\*in terms of polystyrene

The samples supplied in the pellet-shape were dried in a vacuum according to the IUPAC guideline (Dijkstra 2009). For the rheological measurements, the samples were processed into a disk-shape with 25mm in diameter and 1mm in thickness with a hot press machine. The processing temperature was 225°C for PA6 and PA610, and 225°C for PA66. The processing time and the pressure were 5min and 5MPa, respectively. The processed disk-

shaped polyamides were stored in a vacuum oven at 90°C until the measurement. A small amount of the materials was taken from the disk-shaped ones for the thermal analysis before the rheological measurement. For the IR measurement, the film specimens were obtained by the solvent cast from 2,2,2-trifluoroethanol solutions.

## Measurements

The viscoelastic response was measured with a rotational rheometer (Physica MCR301, Anton Paar) in the parallel plate geometry under the nitrogen atmosphere. Before the measurement, we preheated the sample on the rheometer at 250°C for 180min to ensure the steady state (Laun 1979; Ishisaka and Kawagoe 2004). The oscillatory shear was then applied. For the standard viscoelastic measurements at constant temperatures, the strain amplitude was at 1%, and the gap was kept constant during the frequency sweep. For the solidification measurements, the frequency  $\omega$  was held constant, and the loss tangent  $\tan \delta$  was recorded as a function of temperature during the cooling. We applied the normal stress of 0.5 N to eliminate possible slippage during the solidification. Consequently, the gap distance decreased with time. The frequency was  $\omega = 1, 3, 10$ , and 30 rad/s. The cooling rate was fixed at 1.5°C/min unless stated. The choice of these parameters shall be discussed later.

A DSC (Q2000, TA instruments) was used for the thermal analysis. Under the nitrogen atmosphere, for consistency, the samples were subjected to the same thermal history with the rheological measurement. From the measured data, the absolute degree of crystallinity  $\varphi$  was estimated from the enthalpy of crystallization available in the literature (Inoue and Company 1963).

The IR spectra were measured by using an FT-IR spectrophotometer (FT-IR 6100, JASCO) equipped with a temperature controlling system (Model S-100R, ST Japan Inc.). The 16 scanned signals were averaged and recorded with the resolution of 1cm<sup>-1</sup> under the nitrogen atmosphere.

## RESULTS AND DISCUSSION

To determine the adequate range of the frequency  $\omega$  used in the solidification measurements, we measured the melt viscoelasticity. Figure 1 top panel shows the viscoelastic master-curves for PA6/40 and PA6/110 at the reference temperature of 220°C, for example. As shown in the bottom panel, the time-temperature shift-factor  $a_T$  can be reasonably fitted by the Arrhenius form for the examined temperature regime, and the fitting gives the activation energy as 110kJ/mol for PA6/40 and 117 kJ/mol for PA6/110. However, the shift factor for PA6/110 obtained at the highest temperature (leftmost black

circle) apparently deviates from the Arrhenius behavior by unknown reasons. Nevertheless, for the viscoelastic master curves thus obtained, we see that the frequency range used for the solidification measurements,  $\omega = 1, 3, 10,$  and  $30$  rad/s, is not entirely located in the terminal flow regime at the low temperatures. In particular, the frequency  $\omega = 30$  rad/s is not appropriate for the critical gel measurement for some samples, as discussed later. We also note that

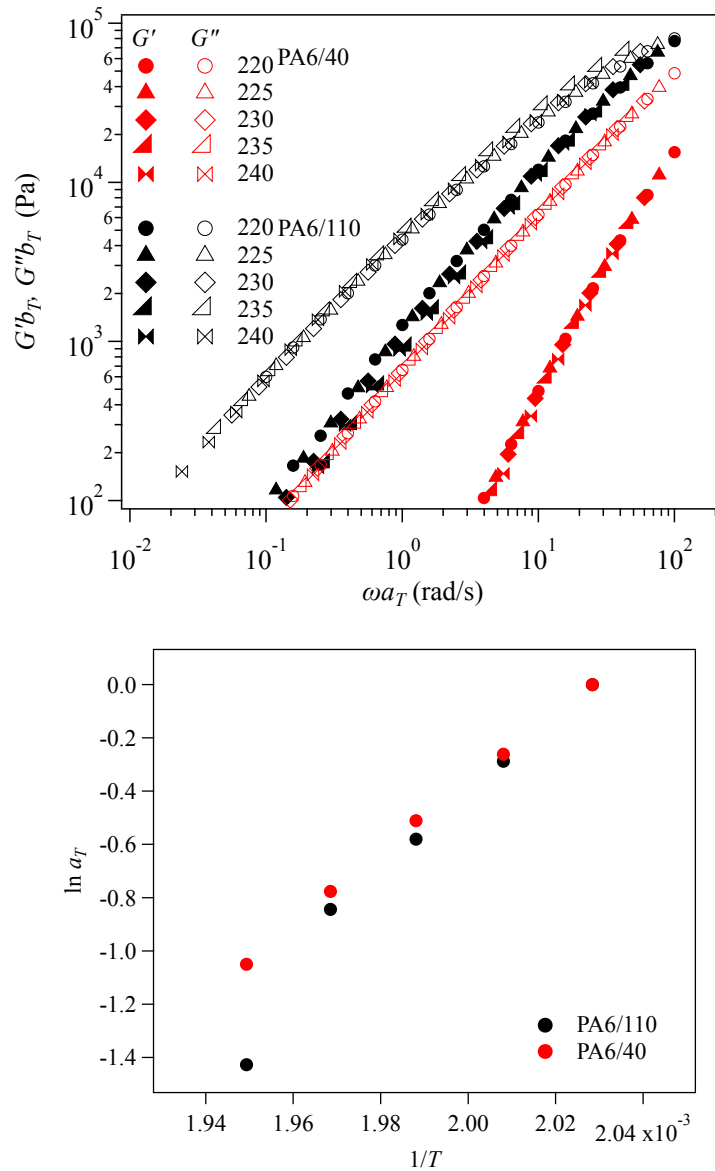


**Figure 1** Viscoelastic master-curves for PA6/40 (red) and PA6/110 (black) at reference temperature of 220 °C (top) and horizontal shift factors plotted against reciprocal temperature (bottom).

Figure 2 shows  $\tan \delta$  measured for PA6/40 under the cooling with the rate of  $1.5^\circ\text{C}/\text{min}$ . As a result of the solidification,  $\tan \delta$  decreased with decreasing the temperature. Though the decreasing behavior of  $\tan \delta$  depends on  $\omega$ , we observe a temperature located around  $201^\circ\text{C}$ , at which  $\tan \delta$  measured with various  $\omega$  cross with each other. This convergence of  $\tan \delta$  suggests the formation of a critical gel at this specific temperature. We thus determined the critical gel temperature  $T_{\text{gel}}$  at the temperature of the  $\omega$ -independent  $\tan \delta$ , and the retardation angle for the critical gel  $\delta_{\text{gel}}$  from the value of the corresponding  $\tan \delta$ . See the vertical and horizontal broken lines in Fig. 2 for the definition of  $T_{\text{gel}}$  and  $\delta_{\text{gel}}$ .

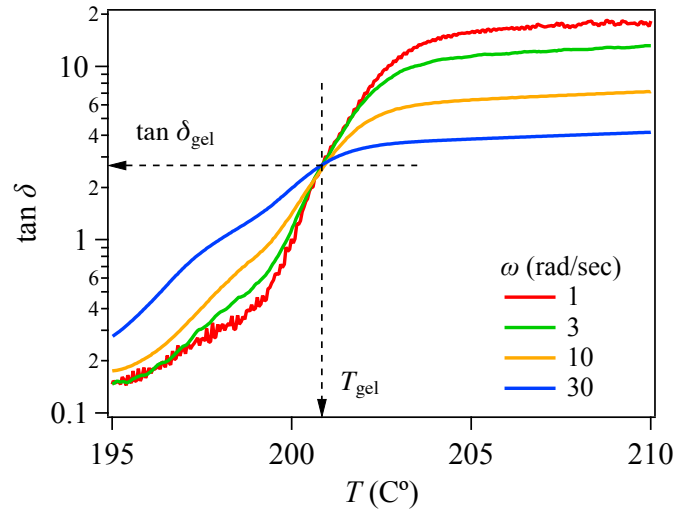


**Figure 2** Development of  $\tan \delta$  for PA6/40 during the cooling at the cooling rate of  $1.5^\circ\text{C}/\text{min}$  for  $\omega = 1, 3, 10$ , and  $30$  rad/s. Broken arrows show  $T_{\text{gel}}$  and  $\delta_{\text{gel}}$  determined from the convergence of  $\tan \delta$ .

Although the observed behavior of  $\tan \delta$  seems reasonable, the convergence of  $\tan \delta$  is not sufficient as the critical gel condition. According to the earlier study (Winter and Mours 1997), for critical gels, both  $G'(\omega)$  and  $G''(\omega)$  are power functions of the frequency  $\omega$  with the same power exponent  $n$ . Besides, the exponent  $n$  is related to the retardation angle  $\delta_{\text{gel}}$  as  $\delta_{\text{gel}} = n\pi/2$ . The  $\omega$  dependence of the moduli is examined in Fig. 3, in which the complex modulus at the critical gel condition  $G_{\text{gel}}^*(\omega)$  is shown for PA6/40 under various cooling rates, and compared with the slope determined from  $\delta_{\text{gel}}$ . At the cooling rates slower than  $4^\circ\text{C}/\text{min}$ ,  $G_{\text{gel}}^*(\omega)$  obeys the expected power-law dependence on  $\omega$ , and the exponent  $n$  (i.e., the slope shown by broken line) is consistent with  $\delta_{\text{gel}}$ . However, at  $5^\circ\text{C}/\text{min}$   $G_{\text{gel}}^*(\omega)$  apparently deviates from the

solid line drawn according to  $\delta_{\text{gel}}$ . This inconsistency implies that the induced mutation at this cooling rate is too fast for the chosen frequency range. Otherwise, the temperature control system of the rheometer may not work correctly.

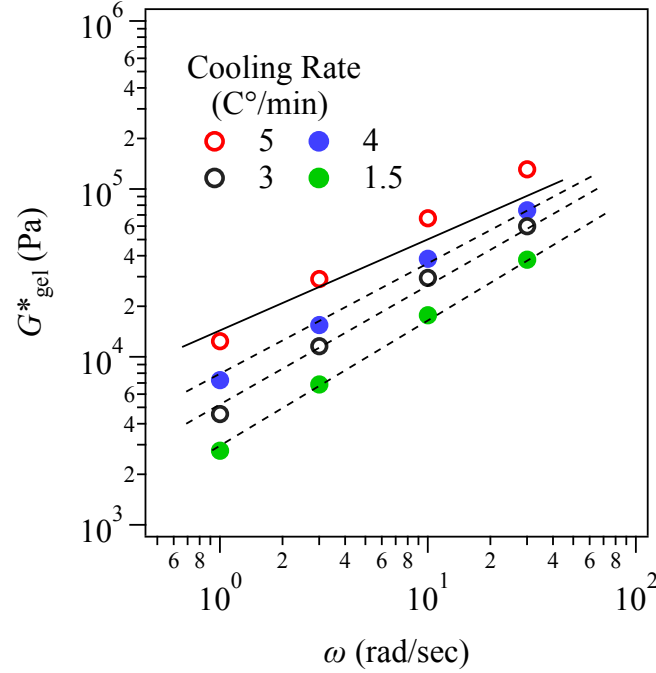


**Figure 3**  $G_{\text{gel}}^*(\omega)$  for PA6/40 under various cooling rates. Solid and broken lines show the power-law behaviors with the exponent determined from  $\delta_{\text{gel}}$ .

Figure 4 shows  $T_{\text{gel}}$  and  $n$  plotted against the cooling rate. The gel stiffness  $S$  obtained from the relation  $G_{\text{gel}}^*(\omega) = S\Gamma(1 - n)\omega^n$ , where  $\Gamma(x)$  is the Gamma function, is also shown. Note that the data for the cooling rates higher than 5°C/min are omitted here because of the inconsistency between the power-law exponent of  $G_{\text{gel}}^*(\omega)$  and the value of  $\delta_{\text{gel}}$  discussed in Fig 3. Fig 4 suggests that the cooling rate does not strongly affect the critical gel structure concerning  $n$  and  $S$ , whereas  $T_{\text{gel}}$  depends on the cooling rate, possibly due to the kinetics of the crystallization. From these results, the cooling rate was fixed at 1.5°C/min for the measurements reported hereafter.

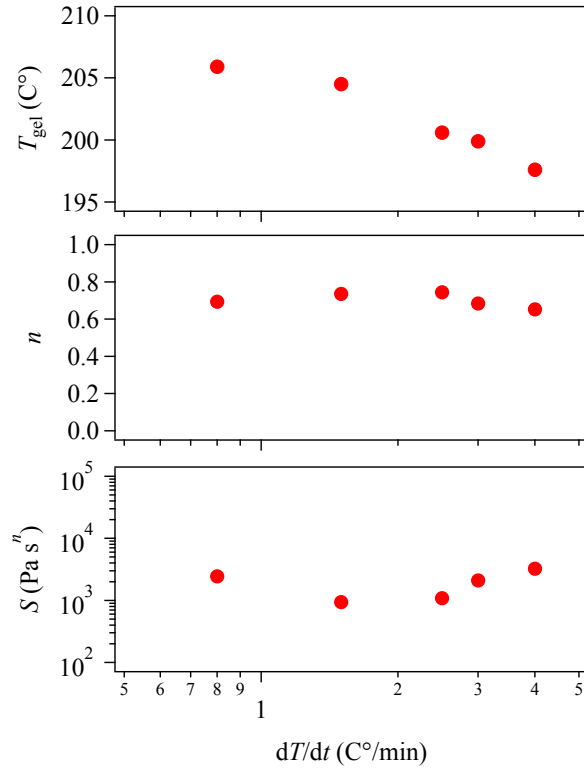


**Figure 4** Cooling rate dependence of the critical gel temperature  $T_{gel}$  (top), the critical exponent  $n$  (mid), and the gel stiffness  $S$  (bottom) for PA6/40.

Because PA6 is semi-crystalline polymer, intuitively, crystallites with a sufficient amount would connect polymers to form the critical gel. To examine this argument, we performed the DSC measurement, and the result is shown in Figure 5 for PA6/40. The heat flow data obtained by DSC measurements generally contain artifacts due to the heat transfer between the sample and the instrument. Following Lopez Mayorga and Freire (Lopez Mayorga and Freire 1987), we deconvoluted the data by assuming a kernel which has a single exponential form. The kernel has one fitting parameter  $\tau$ , which corresponds to the specific heat transfer time. We estimated  $\tau$  from the response to a step temperature change as  $\tau = 8$  sec. We assume that this parameter is the same for all the measurements. From the heat flow data thus corrected, the degree of crystallization  $\varphi_C$  was estimated from the heat of fusion for the crystal reported earlier (Inoue and Company 1963). We note that the obtained  $\varphi_C$  may not be in high accuracy because of the complex crystal formation of PA6 (Sandeman and Keller 1956; Itoh et al. 1975) and ambiguity in the analysis of DSC data.

Nevertheless, the estimated degree of crystallization at the solidification temperature  $\varphi_{gel}$  is smaller than 1%. The degree of crystallinity is significant only at the

lower temperatures than  $T_{\text{gel}}$ . Pogodina and Winter (Pogodina and Winter 1998) reported that for the isothermal solidification of a specific polypropylene sample,  $\varphi_{\text{gel}}$  is ca. 2%. Coppola et al. (Coppola et al. 2006) reported similar results for a poly(1-butene) sample. Our  $\varphi_{\text{gel}}$  seems even smaller than their values.  $\varphi_{\text{gel}}$  was virtually insensitive to the cooling rate for the examined PA6/40.

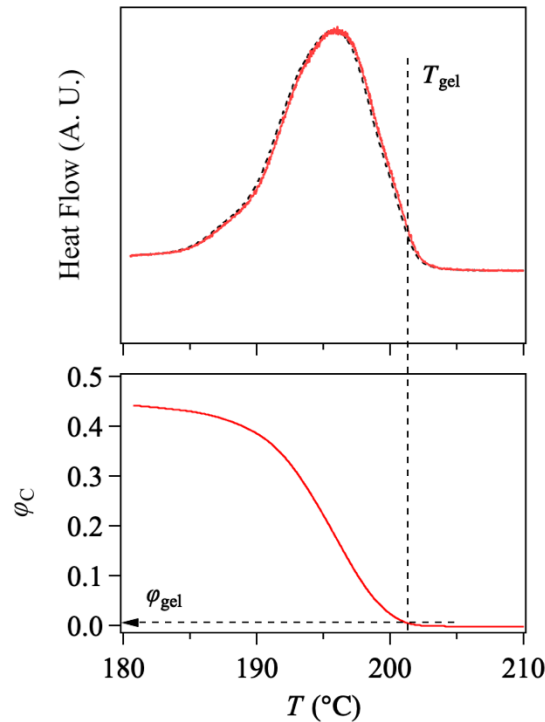


**Figure 5** Heat flow (top) as obtained (dotted curve) and after the deconvolution (solid curve), and the degree of crystallization (bottom) calculated from the deconvoluted data for PA6/40 with the cooling rate of 1.5°C/min. Vertical and horizontal dotted lines indicate  $T_{\text{gel}}$  (obtained from the viscoelastic measurements) and the corresponding  $\varphi_{\text{gel}}$ , respectively.

A possible explanation for the low  $\varphi_{\text{gel}}$  is that the hydrogen bonding may partially stabilize the critical gel of polyamides. To discuss this argument, we measured the IR spectrum of PA6/40 to characterize the critical gel concerning the amount of the hydrogen bonding. We analyzed the absorption peak for the amide I mode (Coleman et al. 1986) located around 1650  $\text{cm}^{-1}$ . According to the earlier study (Skrovanek et al. 1985), the amide I mode is mainly attributable to the C=O stretch mode of carbonyl groups, and there are three different modes: the ordered (1632  $\text{cm}^{-1}$ ), disordered (1652  $\text{cm}^{-1}$ ) hydrogen-bonded groups, and non-hydrogen-bonded free (1680  $\text{cm}^{-1}$ ) groups. Because the peaks by the disordered and free groups are broad and highly overlapped with each

other, discrimination is not trivial. In this work, we decomposed the peaks by assuming that the peak wavenumbers of those two peaks are constant ( $1652\text{ cm}^{-1}$  and  $1680\text{ cm}^{-1}$ ) at the examined temperatures. Although we cannot discuss the peak shifts under such an assumption, we can capture the peak areas. We fitted the amide I mode by the sum of three Voigt functions to determine the peak areas and the peak wavenumber (for the ordered groups) by a house-made fitting code. The fitting-code utilizes the Levenberg-Marquardt method, and the fitting with three peaks worked reasonable as shown in the left panels in Fig 6, where the data (black) almost entirely overlap with the fitting function (yellow). The peak areas were thus calculated from the results of the fitting. From the obtained areas we estimated the fraction of carbonyl groups for each mode by assuming that the molar absorption coefficients are the same with each other. The right panel shows the fractions obtained. From these data, we observe that the contribution of disordered groups (red) is virtually insensitive to temperature. With decreasing the temperature, the number of free groups (blue) decreases whereas that for the ordered groups (green) increases. At the temperatures  $T > T_{\text{gel}}$ , the fractions of ordered and free groups are substantially insensitive to temperature. These data imply that the amount of hydrogen bonds rises around the critical gel temperature in the cooling process. These hydrogen bonds possibly stabilize the critical gel when the crystallinity is small, at least partly. We have also analyzed the N-H stretching mode, which is located around  $3300\text{ cm}^{-1}$ , following Skrovanek et al. (Skrovanek et al. 1985). The result also suggests the formation of hydrogen bonding around  $T_{\text{gel}}$  as shown in Appendix.

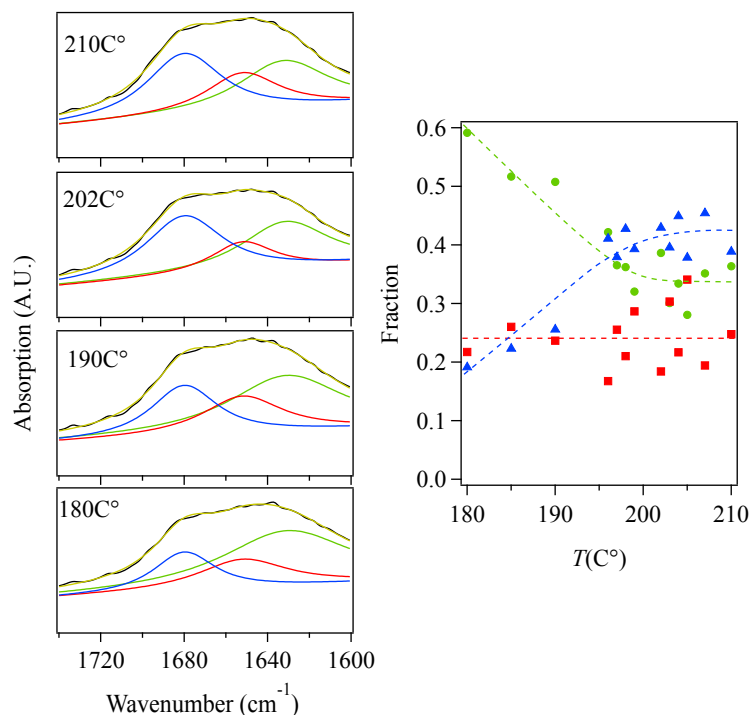


**Figure 6** (Left) FT-IR spectra of PA6/40 in the range of 1600-1740  $\text{cm}^{-1}$  measured at various temperatures. Black and yellow curves are the measured data and the fitting function. Blue, red and green curves are the decomposed Voigt functions. (Right) Fractions of hydrogen-bonded (ordered, disordered) and non-hydrogen-bonded (free) groups calculated from the peak area data. Blue, red and green symbols represent the fractions of the modes shown in the corresponding colors in the left panels. Dotted colored curves are eye-guide.

Thus far, our discussion has been limited to PA6/40, for which the molecular weight is relatively small. To investigate the molecular weight dependence, we performed the solidification measurement and the DSC measurement for PA6 with various molecular weights. The measurements were also conducted for PA66 and PA610 for comparison. The measured  $\tan \delta$  and  $\varphi$  are shown in Fig 7. From these data, we extracted the characteristics of critical gel formation as discussed below.

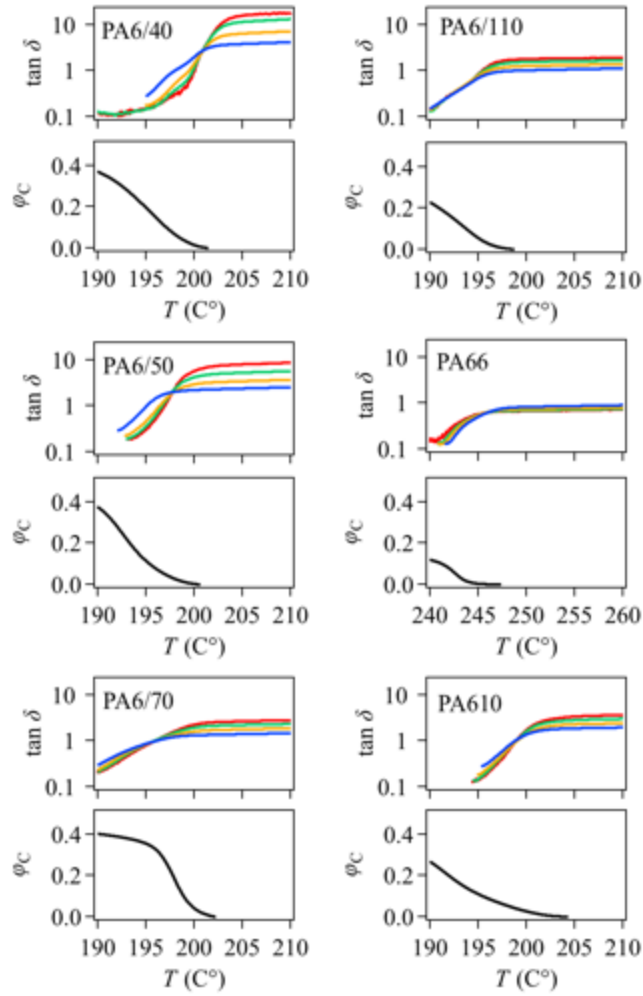


**Figure 7** Development of  $\tan \delta$  and  $\varphi_C$  for various polyamides during the cooling at the cooling rate of  $1.5^\circ\text{C}/\text{min}$ . Blue, yellow, green, and red curves are  $\tan \delta$  for  $\omega = 1, 3, 10,$  and  $30$  rad/s, respectively.

For the obtained data shown in Fig 7, we examined the consistency between  $G_{\text{gel}}^*(\omega)$  and  $\delta_{\text{gel}}$  as shown in Fig 8. As discussed in Fig 4 for PA6/40,  $G_{\text{gel}}^*(\omega)$  basically obeys the power-law behavior with the exponent  $n$  that is consistent with  $\delta_{\text{gel}}$  for all the examined samples. Note however that for  $M_w=70\text{k}$  and  $110\text{k}$  (red triangle and black square in the top panel)  $G_{\text{gel}}^*(\omega)$  deviates from the power-law behavior at the highest frequency. This result implies that the viscoelastic relaxation rate or the mutation rate is lower than the used frequency. In the  $G_{\text{gel}}^*(\omega)$  data, we observe a tendency in which  $n$  decreases and the gel stiffness  $S$  increases with an increase of the molecular weight. Similar molecular weight dependence has been reported for the isothermal solidification of polypropylene (Pogodina and Winter 1998) and poly1-butene (Coppola

et al. 2006). However, for PA6/110, for which the molecular weight is the highest among the examined materials,  $S$  is significantly different from that obtained for the smaller molecular weights. Finally, as shown in the bottom panel,  $G_{\text{gel}}^*(\omega)$  for PA66 and PA610 reasonably obeys the power-law behavior, and  $n$  and  $S$  are similar to those for PA6 with similar molecular weights.

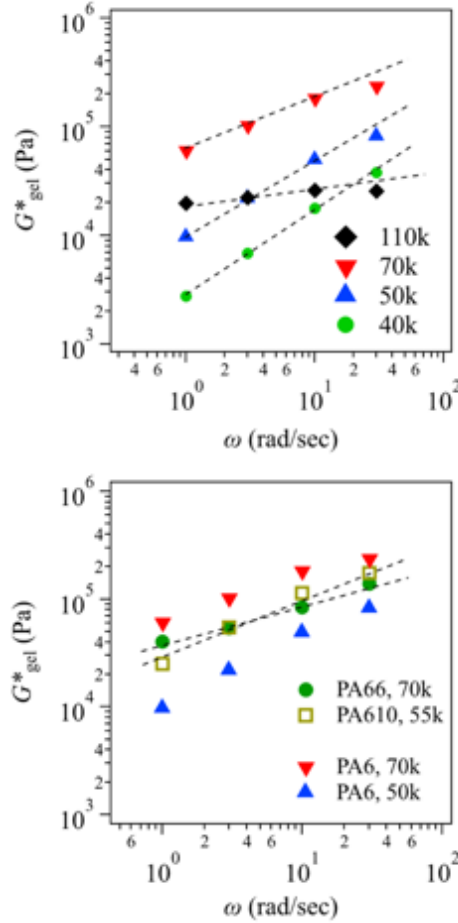


**Figure 8**  $G_{\text{gel}}^*(\omega)$  for PA6 with various molecular weights (top) and PA66 and PA610 (bottom). In the bottom panel, the results for PA6 are also shown for comparison. Broken lines indicate the power-law behavior with the exponent determined from  $\delta_{\text{gel}}$ .

Figure 9 shows the molecular weight dependence of the characteristic measures of the critical gel for PA6. The solidification temperature  $T_{\text{gel}}$  decreases with an increase of the molecular weight (see top panel). Because the thermal behavior observed by DSC does not show clear molecular weight dependence among these samples (see Fig 7), the degree of crystallization  $\varphi_{\text{gel}}$  increases with an increase of the molecular weight (see the second panel). Acierno and Grizzuti (Acierno et al. 2006) have reported that for the isothermal solidification of polycaprolactone,  $\varphi_{\text{gel}}$  is ca. 20%. Our results for PA6/70

and PA6/110 are similar to their value.

The molecular weight dependence of  $T_{\text{gel}}$  and  $\varphi_{\text{gel}}$  implies that long PA chains do not percolate by the hydrogen bonding but by the crystallization. This result is counterintuitive because the hydrogen bonding would suppress the crystallization by the retardation of polymer dynamics, and such a retardation would be significant for long chains. The mechanism of this phenomenon is unknown.

In the second panel,  $\varphi_{\text{gel}}$  of PA66 and PA610 are also indicated for comparison. For the materials with similar molecular weights,  $\varphi_{\text{gel}}$  for PA66 and PA610 is lower than that for PA6. According to the chemistry of the polymers, the amount of hydrogen bonding for PA66 and PA610 is smaller than that for PA6. In this respect, the contribution of hydrogen bonding to the critical gel formation would be less significant than that for PA6. If it is the case,  $\varphi_{\text{gel}}$  for PA66 and PA610 would be larger than that for PA6 since the contribution of crystalline becomes dominant. But the result shown in Fig 9 lies in the opposite direction. We have no clear explanation on the chemistry dependence of  $\varphi_{\text{gel}}$ , although further experiments for PA66 and PA610 with various molecular weights are necessary. The measurements for the other polyamides from PA46 to PA12 would also give further insights.

In the bottom panels in Fig 9, the exponent  $n$  decreases and the stiffness  $S$  increases with increasing molecular weight, as observed for Fig 8. The rise of  $S$  against  $M_w$  can be expressed by a power-law with the exponent of ca. 3.5, if we exclude the result for PA6/110. These behaviors are similar to those reported for the isothermal solidification of polypropylene (Pogodina and Winter 1998) and poly1-butene (Acierno et al. 2002; Coppola et al. 2006). Interestingly, the results for PA66 and PA610 are close to PA6 for  $n$  and  $S$ , probably suggesting structural similarities for their critical gels.

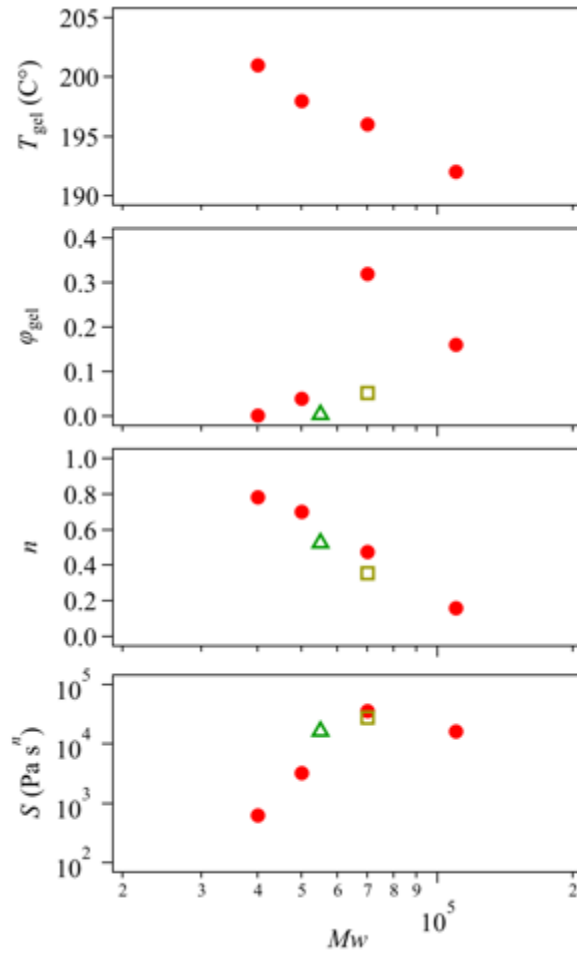


**Figure 9** Molecular weight dependence of  $T_{gel}$ ,  $\phi_{gel}$ ,  $n$ , and  $S$  for PA6 (circle). Data for PA66 (triangle), and PA610 (square) are also shown for comparison.

One may argue that the structural parameters of the critical gels may be related to the amount of crystalline. Figure 10 shows  $n$  and  $S$  plotted against  $\phi_{gel}$  obtained for various cooling rates and molecular weights. For the data collected for PA6 with different molecular weights (circle), there seems a tendency, in which with increasing  $\phi_{gel}$ ,  $n$  decreases whereas  $S$  increases. The PA6/40 data under various cooling rates (cross) are not effectively dispersed in these plots because  $\phi_{gel}$  is virtually insensitive to the cooling rate. The data for PA66 (triangle) and PA610 (square) are shown as well, but these data are different from those for PA6. Overall, there seems no universal correlation between the rheological parameters of critical gels and  $\phi_{gel}$ .

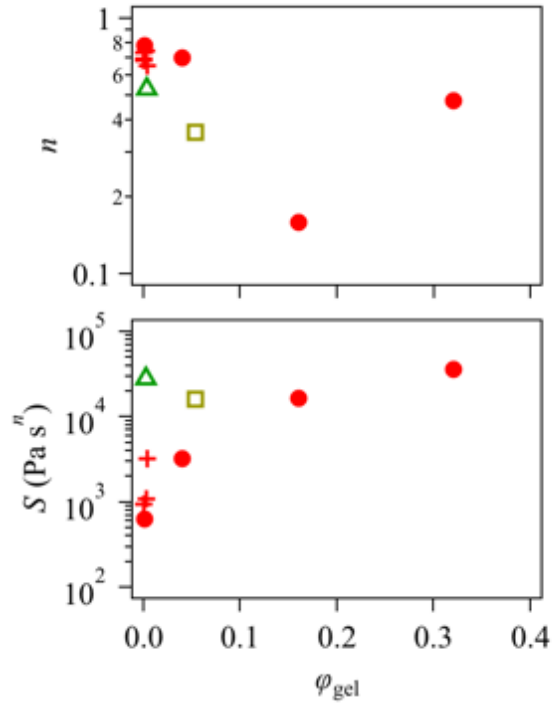


**Figure 10**  $n$  and  $S$  obtained for PA6 under various cooling rates (cross) and with different molecular weights (circle) plotted against  $\phi_{gel}$ . Data for PA66 (triangle) and PA610 (square) are also shown.

An interesting feature for critical gels is the universal relationship between  $n$  and  $S$ . Coppola et al. (Coppola et al. 2006) have reported for poly(1-butene) under the isothermal solidification that the data obtained for various conditions fall on a straight line in the log-linear plot, as shown in Fig 11 (see unfilled circles). Our results for the polyamides show a similar behavior except for the data of PA6/110 (leftmost filled circle), for which  $G_{gel}^*(\omega)$  behavior is significantly different from the others (see Fig 8). In comparison to the earlier data for poly(1-butene), the stiffness  $S$  is smaller for the measured polyamides, whereas the slope for  $\log S$  against  $n$  is interestingly very similar. The mechanism of this universality is unknown. Nevertheless, the consistency with the earlier data for the isothermal solidification supports the validity of our non-isothermal measurements.

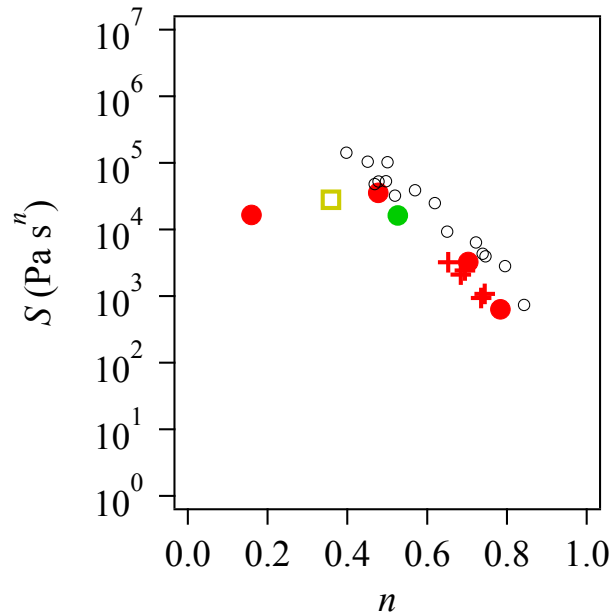


**Figure 11** Relation between  $n$  and  $S$  obtained for PA6 under various cooling rates (cross) and various molecular weights (filled circle). Data for PA66 (triangle), PA610 (square), and for poly(1-butene)(Coppola et al. 2006) (unfilled circle) are also shown.

## CONCLUSIONS

We performed the non-isothermal solidification measurements for polyamides by the Chambon-Winter method for the first time. As reported for the other polymers (mostly under isothermal conditions), polyamides exhibit the solidification via the critical gel formation. For the observed critical gels, the critical exponent and the stiffness reasonably obey the universal relationship, which supports the validity of our measurements. To investigate the effect of crystallization on the critical gel formation, we performed the DSC measurements as well. We found that for PA6 the critical gel temperature decreases, and the crystallinity in the critical gel increases with increasing the molecular weight, and that the crystallinity in the critical gels for PA66 and PA610 seems lower than that for PA6. The FT-IR measurements showed that the amount of hydrogen bonding raises at the critical gel temperature.

The obtained results imply that the critical gels of polyamides are not likely stabilized solely by the crystallization but by the hydrogen bonding, at least partly. In this regard, the naïve idea is that the hydrogen bonding is dominant for polymers with denser amide and carbonyl groups. The hydrogen bonding would also be dominant for long chains, for which the activation energy for the crystal formation is larger than that for

short chains. For the critical gel in which the hydrogen bonding is dominant, the amount of crystalline would be small because the hydrogen bonding for amorphous chains disturbs the crystal formation. However, our results obtained in this study fall in the opposite side. Namely, the crystallinity in the critical gel decreases with a decrease in the density of amide and carbonyl groups and with a reduction of the molecular weight. The mechanism of this counterintuitive results is unknown. Measuring the critical gel temperature, crystallinity, IR spectrum of a series of polyamides (from PA46 to PA12) with different linear density of amide and carbonyl groups for a wide range of molecular weight may provide more conclusive experimental results. Because solubilizing salts and water affect the hydrogen bonding of polyamides (Harings 2009), the effects of these ingredients on the gelation would be interesting as well.

## **Appendix**

Skrovanek et al. (Skrovanek et al. 1985) showed that the peak position of N-H stretching mode, which is located around  $3300\text{cm}^{-1}$ , shifts to lower wavenumber with decreasing the temperature, reflecting the fact that the number of hydrogen bonding increases with decreasing the temperature. Namely, the shift of the peak position results from the fact that the peak is two (or more) overlapping broad absorption peaks at close positions (the absorption peaks of the hydrogen-bonded and free amide groups are at  $3355\text{cm}^{-1}$  and  $3300\text{cm}^{-1}$ , respectively) and the relative magnitudes of the two peaks change with decreasing the temperature. Nevertheless, we observed the peak-shift as shown in the left panel of Fig 12. The wavenumber at the peak is extracted and plotted as a function of temperature in the right panel. The peak-wavenumber decreased with decreasing the temperature, and the magnitude of the decrease is significant across the critical gel temperature, although data points were somewhat scattered.

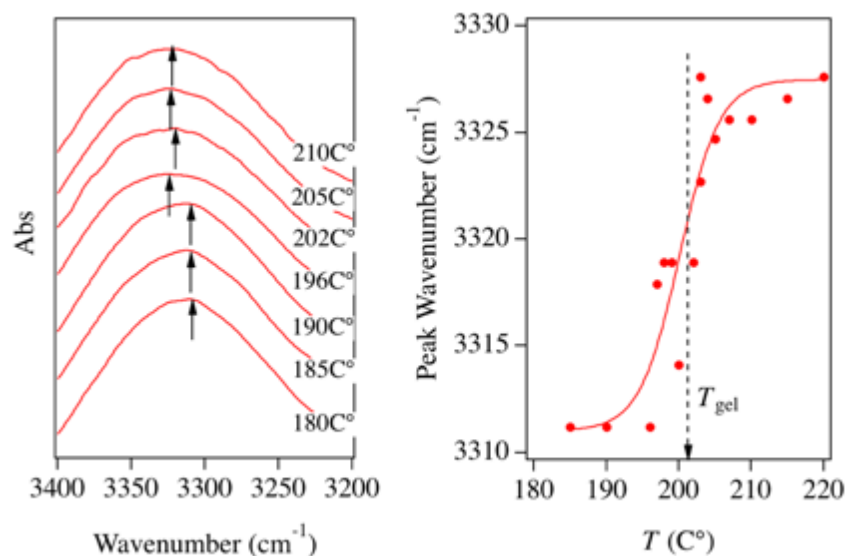


**Figure 12** FT-IR spectra of PA6/40 in the range 3200-3400cm<sup>-1</sup> measured at various temperatures (left), and the peak position of the absorbance spectrum as a function of temperature (right). In the right panel, the vertical dotted line indicates the critical gel temperature obtained from the solidification measurement, and the solid curve is eye-guide.

### Acknowledgment

The authors appreciate the supports from Dr. Yoshifumi Amamoto, Prof. Atsushi Noro, Prof. Atsuhiko Yamanaka, and Prof. Tetsuya Yamamoto. This study is partly supported in part by Grant-in-Aid for Scientific Research (A) (17H01152) from JSPS and by Council for Science, Technology, and Innovation, Cross-ministerial Strategic Innovation Promotion Program, Structural Materials for Innovation from JST.

### References

- Acierno S, Di Maio E, Iannace S, Grizzuti N (2006) Structure development during crystallization of polycaprolactone. *Rheol Acta* 45:387–392. doi: 10.1007/s00397-005-0054-2
- Acierno S, Grizzuti N, Winter HH (2002) Effects of molecular weight on the isothermal crystallization of poly(1-butene). *Macromolecules* 35:5043–5048. doi: 10.1021/ma0200423
- Boutahar K, Carrot C, Guillet J (1998) Crystallization of polyolefins from rheological measurements - Relation between the transformed fraction and the dynamic

- moduli. *Macromolecules* 31:1921–1929. doi: 10.1021/ma9710592
- Chambon F, Winter HH (1987) Linear Viscoelasticity at the Gel Point of a Crosslinking PDMS with Imbalanced Stoichiometry. *J Rheol (N Y N Y)* 31:683. doi: 10.1122/1.549955
- Coleman MM, Skrovanek DJ, Painter PC (1986) Hydrogen bonding in polymers: III further infrared temperature studies of polyamides. *Makromol Chemie Macromol Symp* 5:21–33. doi: 10.1002/masy.19860050104
- Coppola S, Acierno S, Grizzuti N, Vlassopoulos D (2006) Viscoelastic behavior of semicrystalline thermoplastic polymers during the early stages of crystallization. *Macromolecules* 39:1507–1514. doi: 10.1021/ma0518510
- Dijkstra DJ (2009) Guidelines for rheological characterization of polyamide melts (IUPAC Technical Report). *Pure Appl Chem* 81:339–349. doi: 10.1351/PAC-REP-08-07-22
- Fornes TD, Yoon PJ, Keskkula H, Paul DR (2001) Nylon 6 nanocomposites: the effect of matrix molecular weight. *Polymer (Guildf)* 42:09929–09940. doi: 10.1016/S0032-3861(01)00552-3
- Gelfer M, Horst RH, Winter HH, et al (2003) Physical gelation of crystallizing metallocene and Ziegler-Natta ethylene-hexene copolymers. *Polymer (Guildf)* 44:2363–2371. doi: 10.1016/S0032-3861(03)00077-6
- Harings J (2009) Shielding and Mediating of Hydrogen Bonding in Amide-based (Macro)Molecules. Technische Universiteit Eindhoven
- Hess W, Vilgis T a, Winter HH (1988) Dynamical critical behavior during chemical gelation and vulcanization. *Macromolecules* 21:2536–2542. doi: 10.1021/ma00186a037
- Inoue M, Company TR (1963) Studies on Crystallization of High Polymers by Differential Thermal Analysis. *J Polym Sci part A* 1:2697–2709. doi: 10.1002/pol.1963.100010813
- Ishisaka A, Kawagoe M (2004) Examination of the time-water content superposition on the dynamic viscoelasticity of moistened polyamide 6 and epoxy. *J Appl Polym Sci* 93:560–567. doi: 10.1002/app.20465
- Itoh T, Miyaji H, Asai K (1975) Thermal Properties of  $\alpha$ - and  $\gamma$ -Forms of Nylon 6. *Jpn J Appl Phys* 14:206–215. doi: 10.1143/JJAP.14.206
- Izuka A, Winter H, Hashimoto T, et al (1992) Molecular Weight Dependence of Viscoelasticity of Polycaprolactone Critical Gels. 2422–2428. doi: 10.1021/ma00035a020
- Laun HM (1979) Das viskoelastisch Verhalten von Polyamid-6-Schmelzen. *Rheol Acta*

18:478–491

- Lin YG, Winter HH, Mailin DT, Chien JCW (1991) Dynamic Mechanical Measurement of Crystallization-Induced Gelation in Thermoplastic Elastomeric Poly(propylene). *Macromolecules* 24:850–854. doi: 10.1021/ma00004a006
- Lopez Mayorga O, Freire E (1987) Dynamic analysis of differential scanning calorimetry data. *Biophys Chem* 27:87–96
- Mannella GA, La Carrubba V, Brucato V, et al (2011a) No-flow temperature and solidification in injection molding simulation. In: *AIP Conference Proceedings*. pp 689–693
- Mannella GA, La Carrubba V, Brucato V, et al (2011b) No-flow temperature in injection molding simulation. *J Appl Polym Sci* 119:3382–3392. doi: 10.1002/app.32987
- Marchildon K (2011) Polyamides - Still Strong After Seventy Years. *Macromol React Eng* 5:22–54. doi: 10.1002/mren.201000017
- Mours M, Henning Winter H (1995) Viscoelasticity of Polymers during Heating/Cooling Sweeps. *Ind Eng Chem Res* 34:3217–3222. doi: 10.1021/ie00037a006
- Mours M, Winter HH (1994) Time-resolved rheometry. *Rheol Acta* 33:385–397. doi: 10.1007/BF00366581
- Muthukumar M (1989) Screening Effect on Viscoelasticity near the Gel Point. *Macromolecules* 22:4656–4658. doi: 10.1021/ma00202a050
- Muthukumar M, Winter HH (1986) Fractal Dimension of a Cross-Linking Polymer at the Gel Point. *Macromolecules* 19:1284–1285. doi: 10.1021/ma00158a064
- Nichetti D, Cossar S, Grizzuti N (2005) Effects of molecular weight and chemical structure on phase transition of thermoplastic polyurethanes. *J Rheol (N Y N Y)* 49:1361. doi: 10.1122/1.2071987
- Pogodina N V., Lavrenko VP, Srinivas S, Winter HH (2001) Rheology and structure of isotactic polypropylene near the gel point: Quiescent and shear-induced crystallization. *Polymer (Guildf)* 42:9031–9043. doi: 10.1016/S0032-3861(01)00402-5
- Pogodina N V., Winter HH (1998) Polypropylene crystallization as a physical gelation process. *Macromolecules* 31:8164–8172. doi: 10.1021/ma980134I
- Pogodina N V., Winter HH, Srinivas S (1999) Strain effects on physical gelation of crystallizing isotactic polypropylene. *J Polym Sci Part B Polym Phys* 37:3512–3519. doi: 10.1002/(SICI)1099-0488(19991215)37:24<3512::AID-POLB12>3.0.CO;2-#

- Richtering HW, Gagnon KD, Lenz RW, et al (1992) Physical Gelation of a Bacterial Thermoplastic Elastomer. *Macromolecules* 25:2429–2433. doi: 10.1021/ma00035a021
- Sandeman I, Keller A (1956) Crystallinity studies of polyamides by infrared, specific volume and X-ray methods. *J Polym Sci* 19:401–435. doi: 10.1002/pol.1956.120199303
- Schwittay C, Mours M, Winter HH (1995) Rheological expression of physical gelation in polymers. *Faraday Discuss* 101:93. doi: 10.1039/fd9950100093
- Skrovanek DJ, Howe SE, Painter PC, Coleman MM (1985) Hydrogen Bonding in Polymers: Infrared Temperature Studies of an Amorphous Polyamide. *Macromolecules* 18:1676–1683. doi: 10.1021/ma00151a006
- Tanner RI (2002) A suspension model for low shear rate polymer solidification. *J Nonnewton Fluid Mech* 102:397–408. doi: 10.1016/S0377-0257(01)00189-6
- Watanabe K, Nagatake W, Takahashi T, et al (2003) Direct observation of polymer crystallization process under shear by a shear flow observation system. *Polym Test* 22:101–108. doi: 10.1016/S0142-9418(02)00057-0
- Winter HH, Chambon F (1986) Analysis of Linear Viscoelasticity of a Crosslinking Polymer at the Gel Point. *J Rheol (N Y N Y)* 30:367–382. doi: 10.1122/1.549853
- Winter HH, Mours M (1997) Rheology of polymers near liquid-solid transitions. Neutron Spin Echo Spectrosc Viscoelasticity *Rheol* 134:165–234. doi: 10.1007/3-540-68449-2\_3
- Yao Y, Xia X, Mukuze KS, et al (2014) Study on the temperature-induced sol–gel transition of cellulose/silk fibroin blends in 1-butyl-3-methylimidazolium chloride via rheological behavior. *Cellulose* 21:3737–3743. doi: 10.1007/s10570-014-0349-5